SUPPLEMENTARY MATERIALS

I. ESTIMATE OF THE ENERGY DIFFERENCE BETWEEN PROTECTED STATES AND THE MATRIX ELEMENT OF PERTURBATION.

A. Model.

In this section we give the details of the computation of the properties of the studied system which is equivalent to the discrete oscillator described by the Hamiltonian $H = H_0 + H_1$

$$H_0 = -2E_2\cos(2\phi) + E_C(n-n_g)^2. \quad (1)$$
$$H_1 = -E_1\cos\phi \quad (2)$$

We begin with the ideal system described by (1). The two lowest energy states of this problem correspond to wave functions that are non-zero on even or odd charges as explained in the main text. For brevity, we shall refer to these states as odd and even states. In the limit $E_2 \gg E_C$ the splitting of the even and odd states can be found analytically. In this limit the wave functions in the phase representation $\Psi(\phi)$ are mostly localized near the minima of the first term in (1). Quantum transitions between two minima result in the coherent mixture of these two states with the bonding state corresponding to the even and antibonding state to the odd state in charge representation. To prove the correspondence between bonding and even states we notice that the bonding state does not change under the transformation $\phi \to \phi + \pi$, while the antibonding state changes sign under this transformation. In the charge basis this implies that the bonding state has only even components while antibonding - only odd ones. In the quasiclassical approximation the amplitude of this transition in which the phase slips by π is

$$t = A(g)g^{1/2}\exp(-g)\omega_p. \quad (3)$$

Here $A(g) \sim 1$, $\omega_p = 4\sqrt{E_2E_C}$ is the plasma frequency, the dimensionless parameter $g = 4\sqrt{E_2/E_C}$ has a physical meaning of the spread of the wave function in the charge representation: $\langle n^2\rangle = g/4$. In the asymptotic limit of very large $g \gg 1$ the prefactor in (3), $A(g) = \sqrt{\frac{2}{\pi}} \approx 0.8$ but for moderately large g $A(g)$ is significantly different from its asymptotic value as shown in Fig. S1.

The phase slip transitions by $\pm\pi$ lead to the same states. Adding these amplitudes we get $2t\cos\pi n_g$ that gives energy splitting between odd and even states

$$E_{oe} = 4t\cos\pi n_g \quad (4)$$

We now discuss the effect of perturbations. Small but non-zero $E_1\cos\phi$ term in the Hamiltonian leads to the transition between odd and even states. In the limit of large $\langle n^2\rangle \gg 1$ the amplitude of this transition is E_1, so in the basis of odd and even states the Hamiltonian (1) becomes

$$H = \begin{pmatrix} 2t\cos\pi n_g & E_1 \\ E_1 & -2t\cos\pi n_g \end{pmatrix} \quad (5)$$

that gives energy splitting between ground and the first excited state

$$E_{01} = 2\sqrt{E_1^2 + (2t\cos\pi n_g)^2} \quad (6)$$

In deriving this equation we neglected the effect of the higher energy states in each (odd or even) sector, the account of these states lead to the corrections of the order of E_{01}/ω_p. The Hamiltonian $H = H_0 + H_1$ can also be diagonalized numerically, without making these approximation. The difference between the approximate analytical and numerical diagonalization is about 15% for the devices studied in this work.

We now discuss the effect of external noises. The largest source of noise is produced by fluctuating potentials that are coupled to the charge operator. These noises are associated with the fluctuating dipoles in the surrounding dielectrics that lead to both dephasing and decay. The low frequency part of this noise causes the dephasing, it is

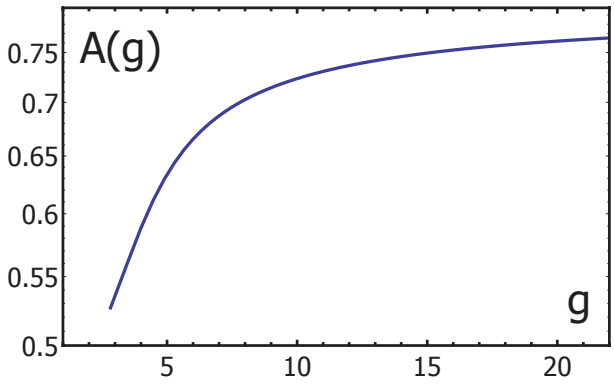

Figure S 1. The dependence of the prefactor A in Eq. (3) on $g = 4\sqrt{E_2/E_C}$. For realistic (not-too-large) values of g, A significantly deviates from its asymptotic value $A(g \gg 1) = \sqrt{\frac{2}{\pi}}$.

usually associated with the incoherently fluctuating two level systems. The high frequency part causes the decay; one can also describe it phenomenologically as the dielectric loss. Another smaller but potentially dangerous source of noise are fluctuations of E_1 caused by flux fluctuations in each rhombus: $\delta E_1 \sim (\delta\Phi/\Phi_0)E_J$ where E_J is the Josephson energy of the small Josephson junction. Generally, the noises can be described as the time variation of the parameters of the Hamiltonian $H = H_0 + H_1$:

$$H_{noise} = V(t)\hat{n} + \delta E_1(t)\cos\phi + \delta E_2(t)\cos 2\phi$$

where $V(t)$ and $\delta E_2(t)$ and $\delta E_1(t)$ are characterized by their spectral densities. Generally, one needs to discuss separately the effects of low and high frequency noises on dephasing and decay and distinguish between charge noise and flux (phase) noise.

B. Charge noise

We begin with the charge noise and the dephasing caused by it. In the charge basis the operator $\hat{n}$ is diagonal, so it remains diagonal in the basis of even and odd states. At $n_g = 0$ the wave functions of these states are symmetric in n, so the potential fluctuations are decoupled in the linear order at $n_g = 0$. For $n_g \neq 0$ the diagonal matrix elements of $\hat{n} - n_g$ can be found by differentiation of E_{oe}:

$$X = (\hat{n} - n_g)_{oo} - (\hat{n} - n_g)_{ee} = \frac{1}{2E_C}\frac{dE_{oe}}{dn_g} = -\frac{2\pi t}{E_C}\sin\pi n_g$$

It contains the same exponential factor as the energy splitting. In the absence of E_1 the external potential leads only to the dephasing proportional to X^2. For instance, the Johnson noise associated with the effective impedance Z of the central island leads to dephasing rate

$$\Gamma_2^Q = \frac{1}{2}M^2\sin^2\pi n_g S_V(\omega_\tau) \tag{7}$$

$$M(g) = \frac{2\pi t}{E_C} = 2\pi A(g) g^{3/2}\exp(-g) \tag{8}$$

$$S_V(\omega) = \omega\coth\left(\frac{\omega}{2T}\right)\frac{\Re Z(\omega)}{Z_Q} \tag{9}$$

Here $Z_Q = \hbar/(2e)^2$ is the quantum of resistance and ω_τ is the typical frequency responsible for dephasing process. For weakly frequency dependent $\Re Z(\omega)$ the main contribution to the dephasing comes from the frequencies $\omega_\tau \sim \Gamma_2$. For realistic temperatures $\Gamma_2 \ll T$ so $S_V = 2T\Re Z/Z_Q$. For non-zero E_1 the energy difference E_{01} is less sensitive to

the charge fluctuations resulting in a somewhat smaller dephasing:

$$\Gamma_2^Q = \frac{1}{2}M^2\left[1-\left(\frac{2E_1}{E_{01}}\right)^2\right]\sin^2\pi n_g S_V(\omega_\tau)$$

We now turn to the decay caused by the charge noise at frequency $\omega = E_{01}$. This off-diagonal matrix element of the charge operator is zero for $E_1 = 0$. Non-zero E_1 mixes odd and even states leading to the decay:

$$\Gamma_1^Q = \frac{1}{2}M^2\left(\frac{2E_1}{E_{01}}\right)^2\sin^2\pi n_g S_V(E_{01}) \tag{10}$$

The important feature of the decoherence and dephasing rates (7,10) is that both of them are zero at $n_g = 0$. This somewhat unusual property is due to the charge symmetry of the wave functions of the logical states. Generally, the Hamiltonian of a device is symmetric under charge inversion which inverses all charges of the device including n_g. This implies that the wave functions of all excited states are odd or even under the charge inversion at $n_g = 0$. Two lowest energy states of the Hamiltonian (1) are even under charge inversion, so the charge matrix elements for these two states are exactly zero.

In order to estimate the value of the dimensionless matrix element M that controls the suppression of the coupling to the charge noise in the experiment it is convenient to express it through the experimentally measurable quantities:

$$M = \frac{\pi}{2}\frac{E_{01}(n_g = 0, \Phi = 0)}{E_{01}(n_g = 0, \Phi = \Phi_0/4)} \tag{11}$$

For the device studied in this work $M \approx 0.5$ leading to a noise suppression factor $\mathcal{P} = 0.5M^2\sin^2\pi n_g < 0.125$ for all values of charge. In order to estimate the decay rate caused by the voltage fluctuations at $n_g \neq 0$ we need to know the magnitude of the effective impedance of the environment $\Re Z$ which is due to the coupling to the transmission line and to the losses in the insulating oxides. The coupling to the transmission line can be estimated by noting that period of the charge oscillations corresponds to $\delta V_L = 3.2$ mV on the transmission line that translates into $\delta V_g = 0.03$ mV giving us an estimate for the coupling $\alpha \sim 10^{-2}$ and $\Re Z(\omega)/Z_Q \sim \alpha^2 \Re Z_L(\omega)/Z_Q \lesssim 10^{-5}$. The intrinsic losses in the insulating oxides comprising good quality Josephson junctions are of the same order: the relaxation rates $\Gamma_1 \sim 1\,\mu s$ observed in quantronium [3, 4] translates into $\Re Z_L(\omega)/Z_Q \sim 10^{-5}$, more recent work [5] reported dielectric losses $\delta \lesssim 10^{-5}$ corresponding to $\Re Z_L(\omega)/Z_Q \lesssim 10^{-5}$ for the resonator made of a long chain of Josephson junction (for the origin of these noises see [1, 2]). This, together with the factor $\mathcal{P}$ results in the quality factor $\omega/\Gamma_1^Q \sim 10^6$ in a rough agreement with the experimental observation at $n_g = 0.5$. We can thus attribute the apparent ~ 30 fold increase in the decay quality factor of the rhombi device to the combination of the modest value of the protection factor, $\mathcal{P} \sim 0.1$ and $(2E_1/E_{01})^2 \sim 0.05$.

C. Flux/phase noise

The magnetic field noise affects the qubit by inducing the fluctuating fluxes in small loops comprising individual rhombi and in the large loop that includes the coupler and controls the phase across the device. We shall refer to the former as rhombi loops and to the latter as the device loop and discuss the effects of these noises separately.

The flux noise in the individual rhombi results in the deviations of the flux from $\Phi_0/2$ that translates into the fluctuations of the energy $E_1(t)$. Generally, the flux noise in a loop can be caused by the local degrees of freedom (spins on the surfaces of superconductors) or by the fluctuations of a global electromagnetic field. Because the area of each rhombus is small, the local flux noise dominates. These fluctuations are characterized by $1/f$ spectrum

$$\langle\delta\Phi(t)\delta\Phi(0)\rangle_\omega = \delta\Phi^2/\omega$$

with $\delta\Phi/\Phi_0 \sim (1-5)\,10^{-6}$, which becomes small at high frequencies, so they cause mostly dephasing (see [7, 8] and references therein for the origin of this noise). The flux directly affect the energy difference between the levels (6). Assuming that flux noise is characterized by the $1/f$ spectrum with the infrared cutoff Ω_0 that translates into the $1/f$ spectrum of E_1 fluctuations

$$\langle\delta E_1(t)\delta E_1(0)\rangle_\omega = \delta E^2/\omega \tag{12}$$

$$\Gamma_2^{\phi} = \sqrt{\frac{\log(E_1/\Omega_0)}{2\pi}} \left(\frac{2E_1}{E_{01}}\right) (2\delta E) \tag{13}$$

Here δE is the typical scale of E_1 fluctuations caused by low frequency noise, it is related to the typical flux variations by $\delta E = \gamma E_{J1}(\delta\Phi/\Phi_0)$ where E_{J1} is the average Josephson energy of the small contact in individual rhombus and $\delta\Phi$ describes the strength of the $1/f$ noise in each rhombi loop:

$$\langle \delta\Phi(t)\delta\Phi(0)\rangle_{\omega} = \delta\Phi^2/\omega$$

Because the effective E_1 of the island is the sum of the contributions from individual rhombi, described by coefficients γ_{R1} and γ_{R2}, the total $\gamma = \gamma_{R1} + \gamma_{R2}$ if the fluxes in two rhombi loops are correlated and the flux in the device loop is integer, so that the noises induced by the flux in different rhombi add. If the flux noises in different loops are independent $\gamma^2 = \gamma_{R1}^2 + \gamma_{R2}^2$. Finally, $\gamma = \gamma_{R1} - \gamma_{R2}$ if the fluxes in different rhombi loops are correlated but the flux in the device loop is half integer, so that their contributions to E_1 cancel each other. For an individual rhombus the numerical coefficient γ_R is somewhat larger than unity in the regime $E_J \gg E_C$: $\gamma_R \approx 3-4$, see Fig.2. We expect approximately $10-20\%$ variations in junction parameters, so the minimal value of $\gamma \approx 0.5$ for half-integer flux in the device loop and perfectly correlated flux noise. Conventional values of the flux noise $\delta\Phi/\Phi_0 \sim (2-5)\,10^{-6}$ imply that expected minimal value of the quality factor due to dephasing achieved at $2E_1 = E_{01}$ is $\omega/\Gamma_1^Q \sim 10^3 - 10^4$ in agreement with experimental observations.

The main effect of the flux fluctuations in the device loops is to modify E_2:

$$\delta E_2(t) = 4\pi E_{2R} \sin(2\pi\Phi/\Phi_0)(\delta\Phi/\Phi_0)$$

This effect, however, becomes small at $\Phi/\Phi_0 = N$ that correspond to maximal $E_2(\Phi/\Phi_0)$. At these fluxes the main effect of the flux noise is due to the $E_1(\Phi/\Phi_0)$ dependence. Below we focus on the origin of the dephasing and decay at these optimal points. Similarly to the noise in each rhombus loop, the low frequency part of the flux noise gives contribution to the dephasing. This contribution is described by the equation similar to (12) with effective δE_{DL} that we can estimate as $\delta E_{DL} \sim E_1(\delta\Phi/\Phi_0)$. Because $E_1 \sim 1-2\,\mathrm{GHz} \ll E_{J1} \approx 60\,\mathrm{GHz}$ this contribution to dephasing is very small compared to that of individual rhombi.

As explained above the dephasing due to the flux noise in the rhombi loops is sensitive to the flux correlations in these loops and the total flux (integer vs. half integer) in the device loop. The study of the dephasing at the different flux values in the device loop can thus provide some information on the flux noise correlations in the adjacent rhombi loops.

Unlike rhombi loops, the device loop is coupled to the external line and to the lossy oxides and experiences significant flux fluctuations at high frequencies. The former fluctuations are directly related to the current fluctuations in the transmission line

$$\langle j(t)j(0)\rangle_{\omega} = \Re Z_{TL}^{-1}(\omega)\omega\coth(\omega/2T)$$

that affects directly the device loop by mutual inductance $M_{TLD} \approx 0.8\,\mathrm{pH}$. Because the mutual inductance is much smaller than the inductance of the coupler, $L_{coup} \approx 0.4\,\mathrm{nH}$ and the effective inductance of the rhombi device, the direct effect of the transmission line on the device is very small

$$\langle \delta E_1(t)\delta E_1(0)\rangle_{\omega} = \left(\frac{E_1'}{E_{TLD}}\right)^2 Z_Q \Re Z_{TL}^{-1}(\omega)\omega\coth(\omega/2T)$$

where $E_1' = dE_1(\varphi)/d\varphi$ and $E_{TLD}/(2\pi\hbar) = 1/(2\pi(2e)^2 M_{TLD}) \approx 2\,10^5$ GHz so that $E_1'/E_{TLD} \approx 10^{-5}$ resulting in a negligible noise for realistic $Z_Q\Re Z^{-1} \sim 10$. The current noise in the transmission line also induces flux noise in LC resonator loop by a larger mutual inductance $M_{TLR} \approx 0.1\,\mathrm{nH}$ that add to the internal noise in the resonator loop due to lossy dielectrics. It is convenient to describe the total dissipation in the resonator by the dimensionless parameter δ that has the physical meaning of the dielectric loss in the capacitor $Z_C = (1-i\delta)/(i\omega C)$. For our resonator $\delta = \Re Z_R \omega C \sim 10^{-3} - 10^{-4}$. The resulting current fluctuations lead to the fluctuations of $E_1(t)$ with the spectrum

$$\langle \delta E_1(t)\delta E_1(0)\rangle_{\omega} = \omega s(\omega)\coth(\omega/2T)$$

where dimensionless function $s(\omega)$

$$s(\omega) = \left(\frac{E_1'}{\hbar\omega_R}\frac{L_{coup}}{L_R(1-\omega^2/\omega_R^2)}\right)^2 \frac{\omega}{\omega_L}\delta. \tag{14}$$

where $\omega_L = 1/L_R(2e)^2 \approx (2\pi)\,40\,\mathrm{GHz}$ and we restored the factors of $\hbar$. These fluctuations give relaxation rate

$$\Gamma_1/E_{01} = s(E_{01})\left[1-\left(\frac{2E_1}{E_{01}}\right)^2\right] \tag{15}$$

Estimating the parameter $E_1'/(2\pi\hbar) \sim 1-2$ GHz and $L_{coup}/L_R \approx 0.1$ we get $s \sim 0.2\,10^{-2}\delta \sim 10^{-6}-10^{-7}$ in rough agreement with the measured quality factor 10^6 for $n_g = 0$. These estimates assumed that the flux in the device loop was chosen in such a way that $E_2(\Phi/\Phi_0)$ is maximal. In practice one minimizes the observed E_{01}which has a contribution of both E_1 and E_2. It is likely that non-zero $dE_2(\varphi)/d\varphi$ at this point gives additional coupling to the flux in the device loop increasing the decay rate. This might be the origin of somewhat smaller quality factors at the optimal point than what expected theoretically.

D. Summary of the effect of the noises

The effect of the charge noise on the device is suppressed by the protection factor $\mathcal{P} = M^2/2$ where M is given by (8) or (11), this factor becomes exponentially small in the limit of large E_2/E_C. It is additionally suppressed by the factors $(2E_1/E_{01})^2$ and $\sin^2\pi n_g$. This makes charge noise and dielectric losses practically irrelevant for these devices at $n_g = 0$ and maximal values of $E_2(\varphi)$ which is the optimal working point of these devices. The magnetic coupling to the low frequency flux noise and to the resonator does not contain exponentially small protection factor $\mathcal{P}$ but it is proportional to E_1^2. The decay rate caused by the coupling to the resonator can be reduced by decreasing this coupling. At the optimal working point the dephasing is caused by the flux noise in individual rhombi loops that induces fluctuations of E_1, it can be suppressed in the structures that contain more rhombi with smaller E_J/E_C.

E. Theoretical expectations of rhombi parameters.

A single ideal rhombus is characterized by the doubly periodic Josephson energy, $E_{2R}\cos 2\phi$ and charging energy E_{CR}. These parameters can be found analytically in the regime of large and small E_{J1}/E_{C1} of individual contacts. Here we define charging energy of individual contact by $E_{C1} = e^2/2C$. In the limit of $E_{J1}/E_{C1} \gg 1$ the second harmonic of the Josephson potential can be found from classical equations, it is linear in E_{J1} :

$$E_{2R} = \frac{16}{15\pi}E_{J1}$$

At small $E_{J1}/E_{C1} \ll 1$ it appears only in the fourth order of the perturbation theory in (E_{J1}/E_{C1}):

$$E_{2R} = \frac{7}{128}\left(\frac{E_{J1}}{E_{C1}}\right)^4 E_{C1}$$

The crossover between two regimes happens at $E_{J1}/E_{C1} \sim 5$ as shown in Fig. 2. The effective capacitance of the rhombus with $E_{J1}/E_{C1} \ll 1$ is equal to the capacitance of a single junction $C_R \approx C$, at larger $E_{J1}/E_{C1} \gtrsim 1$ the charge spreads out across the rhombi resulting in the increase of the effective capacitance to $C_R \approx 2-3\,C$ for the relevant range of the $E_{J1}/E_{C1} = 3-8$.

The junctions of the device shown in this work were expected to have $E_{J1} \approx 60\,\mathrm{GHz}$ and $E_{C1} \approx 15\,\mathrm{GHz}$ that give $E_{2R} = 12\,\mathrm{GHz}$ which is very close to the fitted value of $E_2 = 8.5$ GHz. The expected value of the charging energy $E_C = e^2/C_R \approx 10-15$ GHz that is also close to the fitted value $E_C = 15\,\mathrm{GHz}$. The agreement is especially good if one takes into account very fast dependence of $E_2(E_{J1}/E_{C1})$ in this range.

Small deviations of the flux from the half quantum lead to the appearance of the first harmonic of the Josephson potential, $\delta E(\phi) = E_1(\delta\Phi)\sin\phi$. In the quasiclassical limit $E_{J1}/E_{C1} \gg 1$

$$E_1(\delta\Phi) = \frac{16}{3}E_{J1}\frac{\delta\Phi}{\Phi_0}.$$

For moderate values of $E_{J1}/E_{C1} = 3-8$ the numerical coefficient in this equation is somewhat less as shown in Fig. 2.

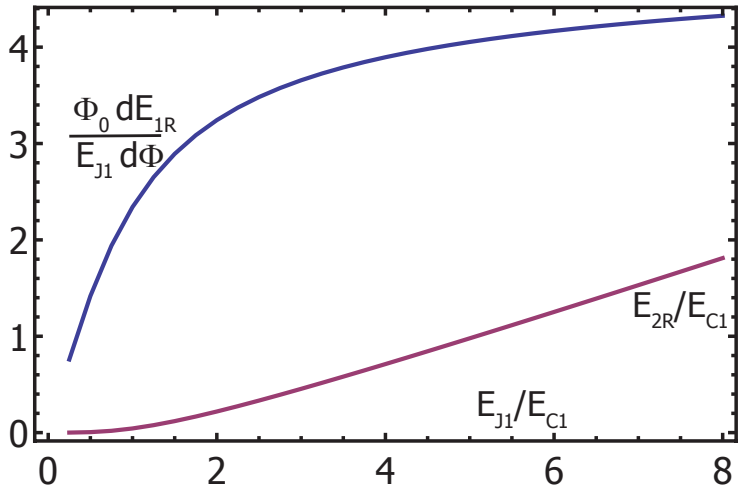

Figure S 2. Dependence of rhombi parameters on the properties of single junctions. The upper (blue) curve shows the sensitivity to the flux variations, the lower curve gives the strength of the doubly periodic potential.

II. MEASUREMENT SETUP AND PROCEDURES.

The main elements of the MW set-up are shown in Fig. S3. The microwave response of the Josephson rhombi chain coupled to the read-out LC resonator (see Fig. 2) was probed by measuring both the phase and amplitude of the microwaves traveling along a microstrip feedline coupled to the resonators. This setup enabled the testing of several devices fabricated on the same chip in a single cooldown.

The microwaves at the probe frequency ω_1, generated by a microwave synthesizer, were coupled to the cryostat input line through a 16 dB coupler and transmitted through the microstrip line coupled to the LC resonators. The cold attenuators and low-pass filters in the input microwave lines prevent leakage of thermal radiation into the resonator. On the output line, two cryogenic Pamtech isolators ($\sim$ 36 dB isolation between 3 and 10 GHz) anchored to the mixing chamber attenuate the 5 K noise from the cryogenic HEMT amplifier (Caltech CITCRYO 1-12, 35 dB gain between 1 and 12 GHz). The amplified signal is mixed by mixer M1 with the local oscillator signal at frequency ω_r, generated by another synthesizer. The intermediate-frequency signal $A(t) = A\sin(\Phi t+\phi)+noise$ at $\Phi \equiv (\omega_1-\omega_r)/2\pi = 30MHz$ is digitized by a 1 GS/s digitizing card (AlazarTech ATS9870). The signal is digitally multiplied by $\sin(\Omega t)$ and $\cos(\Omega t)$, averaged over an integer number of periods, and its amplitude A (proportional to the microwave amplitude $|S_{21}|$) and phase ϕ is extracted as $A = \sqrt{\langle (A(t)sin\Omega t)^2\rangle + \langle (A(t)cos\Omega t)^2\rangle}$ and $\phi = \arctan\left[\frac{\langle (A(t)sin\Omega t)^2\rangle}{\langle (A(t)cos\Omega t)^2\rangle}\right]$, respectively. The reference phase ϕ_0 (which randomly changes when both ω_1 and ω_r are varied in measurements) is found using similar processing of the low-noise signal provided by mixer M2 and digitized by the second channel of the ADC. This setup enables accurate measurements of small changes $\phi-\phi_0$ unaffected by the phase jitter between the two synthesizers. The low noise of this setup allowed us to perform measurements at a microwave excitation level of -133 dBm which corresponded to a sub-single-photon population of the tank circuit. In the second-tone measurements, the tested rhombi chain was excited by the microwaves at frequency ω_2 coupled to the transmission line via a 16 dB coupler.

In the presence of charge fluctuation on the central island of the chain, we have applied a sweep-by-sweep averaging method. Since these fluctuations are slow (on the time scale of seconds), we perform 10-100 full-range sweeps of the second tone frequency (at a rate of 10ms per one value of ω_2) and then perform averaging of the completed sweeps rather than a point-by-point averaging of the second tone sweep.

The sample was mounted inside an rf-tight copper box that provided the ground plane for the microstrip line and LC resonator. This box was placed inside another rf-tight copper box in order to eliminate any stray infrared photons. This nested-box construction was housed inside a cryogenic magnetic shield (A4k), followed by a superconducting aluminum magnetic shield. All the connectors inside the magnetic shields were non-magnetic (EZForm); this reduced the stray magnetic field at the sample location down to 0.1 mGauss. The entire sample and shielding construction was anchored to the mixing chamber of a cryogen-free dilution refrigerator with a base temperature of 20 mK.

In order to control the charge on the central island of the chain, a DC gate voltage was applied to the microstrip

line via a bias-T. External noises at the DC port of the bias-T were attenuated with a voltage divider and a series of low-pass filters and stainless steel powder filters.

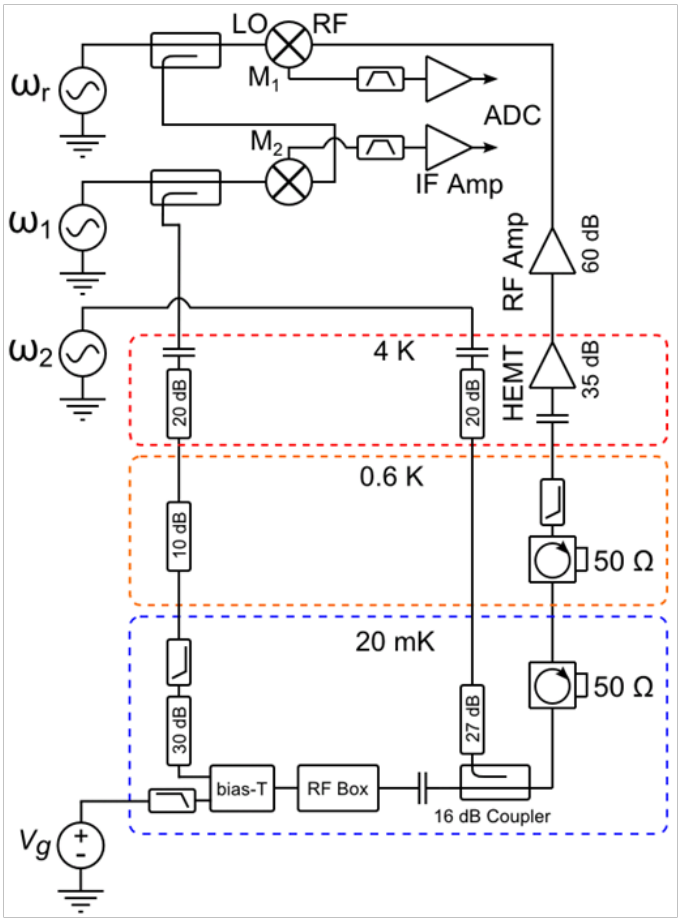

Figure S 3. Simplified circuit diagram of the measurement setup. The microwaves at the probe frequency ω_1 are transmitted through the microstrip line inductively coupled to the rhombi chain and the LC resonator located inside the rf sample box. The microwaves at ω_r, after mixing with the microwaves at ω_1, provide the reference phase ϕ_0. The signal at ω_1 is amplified, mixed down to an intermediate frequency $\omega_1 - \omega_r$ by mixer M2, and digitized by a fast digitizer (ADC). The microwaves at the second-tone frequency ω_2 were used to excite the $|0\rangle - |1\rangle$ transitions in the qubit.

III. THE PROBE-TONE MEASUREMENTS

The oscillations in the LC resonance frequency versus the magnetic flux are shown in Fig. S3 near zero magnetic field (a) and full frustration $\Phi_R = \Phi_0/2$ (b). The oscillations in the LC resonance frequency reflect the dependence of the inductance of the chain in its ground state as a function of the phase across the chain, $\varphi = 2\pi\Phi/\Phi_0$. Near full frustration, the period of oscillations corresponds to $\Delta\varphi = \pi$. The range of fluxes where the π-periodicity was observed agrees well with the theory. The dependence $|S_{21}|(\varphi)$ also demonstrates avoided crossings observed when the resonance frequency f_{01} coincides with the resonance in the read-out LC resonator (the "spikes" in Fig. S3b), but the second-tone measurements discussed in the main text provide much more detailed information on the chain spectrum.

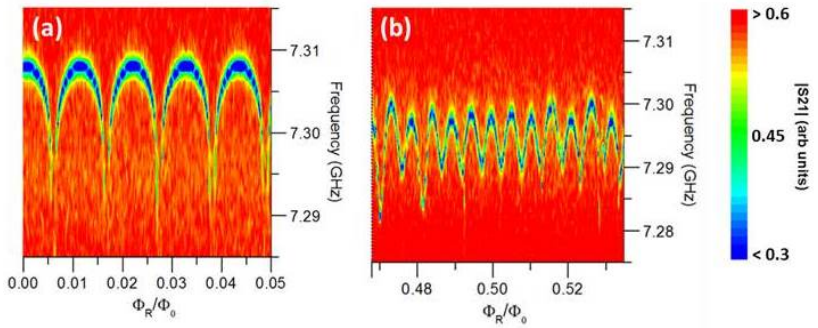

Figure S 4. The color-coded plots show the transmission microwave amplitude $|S_{21}|$ versus the probe-tone microwave frequency and the phase across the chain (in units of rhombi flux) near zero field (a) and near full frustration $\Phi_R = \Phi_0/2$ (b). The period of the inductance oscillations changes from $\Delta\Phi = \Phi_0$ ($\Delta\varphi = 2\pi$) to $\Delta\Phi = \Phi_0/2 (\Delta\varphi = \pi)$ near full frustration.

The energy E_2 can be estimated from the measurements of the probe-tone microwave amplitude $|S_{21}|$ versus the magnetic flux. The energy E_2 is inversely proportional to the Josephson inductance L_J of the chain: $E_2 = (\frac{\Phi_0}{4\pi})^2 \frac{1}{L_J}$. Both quantities depend on the phase across the chain - $E_2(\varphi) = E_2 \cos(2\varphi)$, $L_J = L_{J0}/\cos(2\varphi)$ - so $E_2 \to 0$ and $L_J \to \infty$ when $\varphi \to \pi/2$. Using the equivalent circuit in Fig. 2c, one can estimate L_{J0} from the swing of the resonance frequency of the LC resonator coupled to the chain (10 MHz in Fig. S4b). Using $L = 3nH$ and $L_C = 0.4nH$, we estimate $L_{J0} = 19nH$, which translates into $E_2 = 0.39K$ (or 7.7 GHz). This estimate agrees very well with the fitting parameters used to simulate the chain spectrum.

IV. SPECTROSCOPIC DATA AT $n_g = 0$ AND $n_g = 0.5$

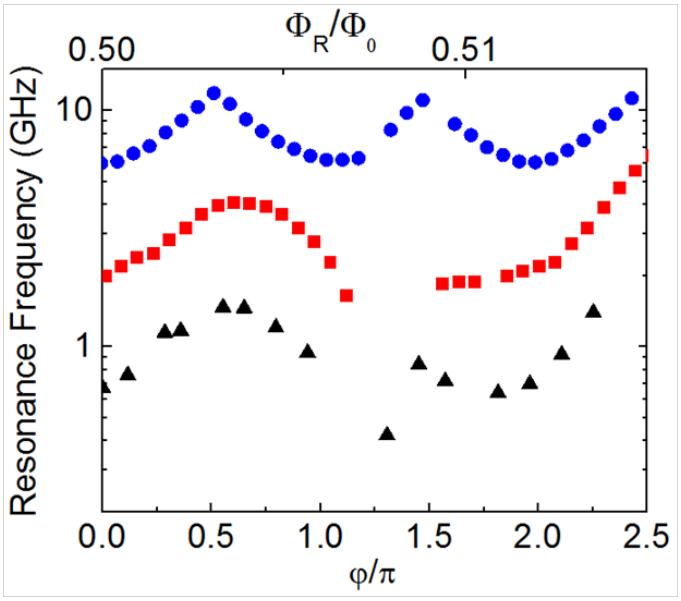

Figure S 5. The dependences of the resonance frequency f_{01} on the phase φ across the chain near full frustration at $n_g = 0$ (blue dots) and 0.5 (red squares). For comparison, $E_1(\varphi)$ is shown on the same plot (black triangles).

V. RABI OSCILLATION MEASUREMENTS

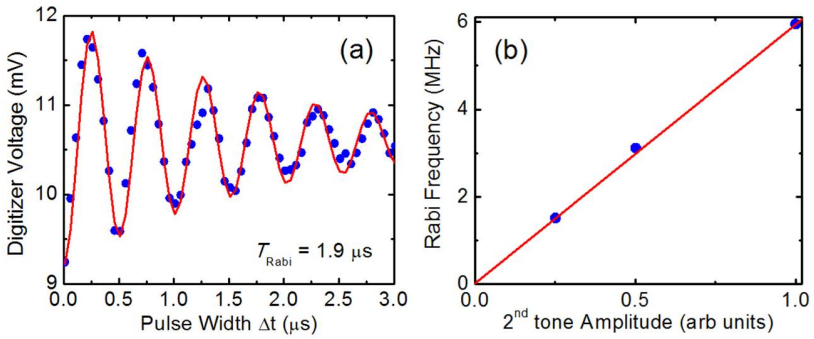

Figure S 6. (a) Rabi oscillations of the population of the first excited level (measured by the digitizer) vs. the second-tone pulse width (blue dots), and a fit (exponentially damped sinusoidal oscillations) with a decay time of 1.9 μs (red line). (b) Measured Rabi frequency vs. the second-tone pulse amplitude (blue dots) and a linear fit (red line).

Time domain measurements were performed in a similar manner as described in Ref. [1]. For measurements of Rabi oscillations shown in Fig. S6(a), a short microwave spectroscopy pulse of the width Δt with Gaussian-shaped rising and falling edges was applied to the Rhombi qubit in its ground state at a repetition rate of 2 kHz. At the end of the spectroscopy pulse a 3μs measurement tone pulse was applied to the LC resonator followed by the digitizer measurement which was delayed by 0.5 μs from the beginning of the measurement-tone pulse to allow sufficient damping of "ringing" in the LC resonator. This measurement was repeated 3×10^4 times and averaged for each Δt. The signal-to-noise ratio (SNR) with this averaging and an interrogation time of 0.5 μs is approximately 20, which would correspond to a SNR of 0.1 for a single-shot measurement with the current setup. Measurements of the Rabi frequency vs. the second-tone pulse amplitude (Fig. S6(b)) confirm the expected linear dependence of the Rabi frequency on the second-tone pulse amplitude within the amplitude range used throughout the time-domain measurements discussed in this paper. The Rabi measurement data was used to determine the width of a π pulse in the spin echo and Ramsey measurements. Measurements of Ramsey and spin echo decay times were performed in a similar manner with the second-tone frequency in resonance with the qubit.

[1] J. Martinis, R. McDermott, M. Steffen, M. Ansmann, K. Osborn, K. Cicak, S. Oh, D. Pappas, R. Simmonds and C. Yu. Phys. Rev. Lett., **95**, 210503 (2005).
[2] L. Faoro and L. B. Ioffe. Phys. Rev. Lett. **109**, 157005 (2012).
[3] D. Vion, A. Aassime, A. Cottet, P. Joyez, H. Pothier, C. Urbina, D. Esteve, and M. H. Devoret. Science **296**, 866 (2002).
[4] M. Metcalfe, E. Boaknin, V. Manucharyan, R. Vijay, I. Siddiqi, C. Rigetti, L. Frunzio, R. J. Schoelkopf, and M. H. Devoret. Phys. Rev. B **76**, 174516 (2007)
[5] N. A. Masluk, Ioan M. Pop, A. Kamal, Zl. K. Minev, and M. H. Devoret. Phys. Rev. Lett. **109**, 137002 (2012).
[6] A. Wallraff, D. I. Schuster, A. Blais, L. Frunzio, J. Majer, M. H. Devoret, S. M. Girvin, and R. J. Schoelkopf. Phys. Rev. Lett. **9**5, 060501 (2005).
[7] S. Sendelbach, D. Hover, A. Kittel, M. Mï¿œck, John M. Martinis, and R. McDermott. Phys. Rev. Lett. 100, 227006 (2008).
[8] L. Faoro and L. Ioffe. Phys. Rev. Lett. **100**, 227005 (2008).